Shadowing in neutrino deep inelastic scattering and the determination of the strange quark distribution

C. Boros
Department of Physics and Mathematical Physics, and Special Research Center for the Subatomic Structure of Matter, University of Adelaide, Adelaide 5005, Australia

J. T. Londergan
Department of Physics and Nuclear Theory Center, Indiana University, Bloomington, Indiana 47404

A. W. Thomas
Department of Physics and Mathematical Physics, and Special Research Center for the Subatomic Structure of Matter, University of Adelaide, Adelaide 5005, Australia

(Received 27 April 1998; published 6 November 1998)

We discuss shadowing corrections to the structure function F_2 in neutrino deep-inelastic scattering on heavy nuclear targets. In particular, we examine the role played by shadowing in the comparison of the structure functions F_2 measured in neutrino and muon deep inelastic scattering. The importance of shadowing corrections in the determination of the strange quark distributions is explained. [S0556-2821(98)01323-X]

PACS number(s): 13.60.Hb, 11.40.Ha, 12.40.Vv, 13.15.+g

I. INTRODUCTION

Comparisons of structure functions measured in different reactions have always been very useful in investigating the structure of hadrons and extracting the parton distribution functions. Recently, there has been much interest in the measurement of the structure function $F_2^{\nu}(x,Q^2)$ in neutrino deep inelastic scattering by the CCFR Collaboration [1]. This measurement makes it possible to compare structure functions measured in neutrino-induced reactions with those measured in charged lepton-induced ones and hence to test the universality of parton distribution functions and to extract the strange quark density of the nucleon.

The CCFR Collaboration compared the neutrino structure function $F_2^{\nu}(x,Q^2)$ extracted from their data on an iron target [1] with $F_2^{\mu}(x,Q^2)$ measured for the deuteron by the New Muon Collaboration (NMC) [2]. In the region of intermediate values of Bjorken x $(0.1 \leqslant x \leqslant 0.4)$, they found very good agreement between the two structure functions. In the small x-region however $(x<0.1)$, the CCFR group found that the two structure functions differ by as much as 10–15%. Since several corrections have to be taken into account in order to compare the structure functions $F_2^{\nu}(x,Q^2)$ and $F_2^{\mu}(x,Q^2)$, the apparent discrepancy between the structure functions at small x depends on the validity of the assumptions made in correcting the data. One of the crucial points is that the neutrino structure function is measured on an iron target, while the muon data is taken on the deuteron. Thus, one has to account for heavy target effects in the neutrino reactions. In applying these corrections to the data, it has been assumed that heavy target effects are the same in neutrino and muon deep inelastic scattering, and a parametrization obtained from muon data has been used.

A priori there is no reason *why* heavy target corrections in neutrino deep inelastic scattering should be the same as those in charged lepton deep inelastic scattering. Therefore, we feel that it is important to investigate the role played by shadowing in neutrino reactions *before* concluding that the two structure functions are *really* different in the small x-region. Furthermore, there are additional uncertainties arising because the heavy target corrections are applied by parametrizing *only* the x-dependence of the available data on the ratio $R \equiv F_2^{\mu A}(x,Q^2)/F_2^{\mu D}(x,Q^2)$ between the neutrino structure function measured on heavy targets and that of the deuteron from charged lepton deep inelastic scattering. However, it is well known that shadowing corrections are very much Q^2 dependent for smaller Q^2 values (where a considerable part of the available data was taken), and the Q^2 and x-dependence of the data are strongly correlated because of the fixed target nature of these experiments.

In view of these uncertainties, the main objective of this paper is a careful re-analysis of the shadowing corrections which must be understood before one can attribute the discrepancy between $F_2^{\nu}(x,Q^2)$ and $F_2^{\mu}(x,Q^2)$ to other possibilities, such as to different strange quark and anti-strange quark distributions [3–7], to higher order QCD-corrections [8–10] or to the violation of charge symmetry in parton distribution functions [11–15].

II. COMPARISON OF NEUTRINO AND MUON STRUCTURE FUNCTIONS

Comparisons of structure functions measured in neutrino deep-inelastic scattering with those measured in charged lepton deep-inelastic scattering are based on the interpretation of these structure functions in terms of parton distribution functions in the quark parton model. Assuming the validity of charge symmetry and neglecting the contributions from charm quarks, the structure functions $F_2^{\nu N_0}(x,Q^2)$ and $F_2^{\mu N_0}(x,Q^2)$ on iso-scalar targets (N_0) are given by the following expressions:

$$F_2^{\mu N_0}(x)=\tfrac{5}{18}x[u(x)+\overline{u}(x)+d(x)+\overline{d}(x)+\tfrac{2}{5}(s(x)+\overline{s}(x))] \tag{1}$$

$$F_2^{\nu N_0}(x)=x[u(x)+\overline{u}(x)+d(x)+\overline{d}(x)+2s(x)]. \tag{2}$$

Thus, they can be related to each other by

$$F_2^{\mu N_0}(x,Q^2)=\frac{5}{18}F_2^{\nu N_0}(x,Q^2) - \frac{3x[s(x)+\overline{s}(x)]+5x[s(x)-\overline{s}(x)]}{18}. \tag{3}$$

This means that, once the charged lepton and neutrino structure functions and the strange quark distributions are known, one can test the validity of this relation, or one can use the above relation to extract the strange quark distribution from the measured structure functions.

The recent measurement of the structure function F_2^{ν} by the CCFR Collaboration [1] makes it possible to carry out such an analysis for the first time with reasonable precision. However, the actual comparison between neutrino and charged lepton structure functions is not straightforward because several corrections have to be applied to the data. Since the above relations are only valid for Q^2 values well above charm production threshold, charm threshold effects have to be removed. Furthermore, the neutrino structure function has been extracted from measurements using an iron target. Therefore one has to account for the excess of neutrons in iron (iso-scalar corrections) and for heavy target effects.

In applying the heavy target corrections, one could assume that heavy target effects are the same in *neutrino* deep inelastic scattering as in *muon* deep inelastic scattering and use a parametrization of the heavy target corrections obtained from muon-induced reactions. This is the assumption which has been made by the CCFR Collaboration in its analysis [1]. Using such a parametrization for the heavy target correction and a parametrization of the strange quark distribution [16] extracted from other experiments, we calculated the ''charge ratio'':

$$R_c(x)\equiv\frac{F_2^{\mu N_0}(x)}{(5/18)F_2^{\nu N_0}(x)-x(s(x)+\overline{s}(x))/6} \approx 1-\frac{s(x)-\overline{s}(x)}{Q_s(x)}. \tag{4}$$

Here, we defined $Q_s(x)\equiv\Sigma_{q=u,d,s}[q(x)+\overline{q}(x)]-3(s(x)+\overline{s}(x))/5$. For the charged lepton structure function, we used $F_2^{\mu N_0}$ measured in muon deep inelastic scattering by the NMC Collaboration on a deuteron target [2]. For fixed x-values, we averaged the structure function over the overlapping Q^2-regions of the two experiments in order to obtain better statistics. We also applied a cut for Q^2 less than 3.2 GeV^2 and 2.5 GeV^2 for the CCFR data and the NMC data, respectively, in order to insure the validity of quark-parton model relations. For the strange quark distributions, we used the CTEQ (CTEQ4L) distributions of Lai *et al.* [16].

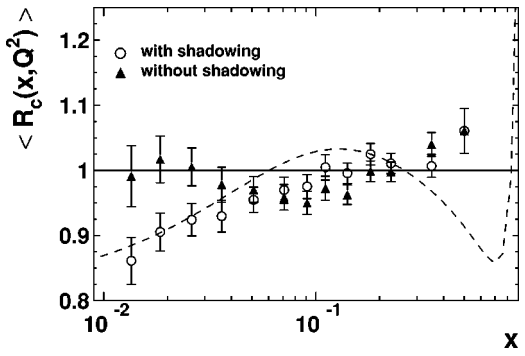

FIG. 1. The ''charge ratio'' R_c of Eq. (4) as a function of x calculated using the CCFR [1] data for neutrino and NMC [2] data for muon structure functions. The data have been integrated over the overlapping kinematical regions and have been corrected for heavy target effects using a parametrization (dashed line) for heavy target corrections extracted from charged lepton scattering. The result is shown as open circles. The ratio obtained without heavy target corrections is shown as solid triangles. Statistical and systematic errors are added in quadrature.

The result is shown in Fig. 1. We note that, under the assumptions that $s(x)=\overline{s}(x)$ and that charge symmetry is valid for parton distributions, the ''charge ratio'' R_c of Eq. (4) should be equal to one at all x. For intermediate values of Bjorken x $(0.1\leqslant x\leqslant 0.4)$, the charge ratio R_c is equal to one to within errors of a few percent. The agreement between the two structure functions in this x region allows us to place rather strong upper limits on contributions from charge symmetry violation in parton distributions [13]. However, R_c appears to be substantially below unity in the small-x region, for $x<0.1$.

In Fig. 1 we also show the effects of the heavy target corrections which were applied to the neutrino structure functions. The solid triangles show the result we would obtain for the ''charge ratio,'' if we did not apply any heavy target corrections to the neutrino structure functions. We see that the heavy target corrections definitely play a very important role in interpreting the result of such an analysis. Since the heavy target corrections applied to the neutrino results were obtained from data in charged lepton deep-inelastic scattering, differences between shadowing for neutrinos and for muons could make a substantial difference in the charge ratio R_c in Eq. (4). Since the heavy target corrections for large x-values are expected to be independent of the probe used to measure the quark distributions in a nucleus (at large x the target corrections should be dominated by quark Fermi motion), in this paper we discuss only the shadowing region, $x\leqslant 0.1$.

III. SHADOWING CORRECTIONS

In calculating the shadowing corrections, we use a two-phase model which has been successfully applied to the description of shadowing in charged-lepton deep inelastic scattering [17,18]. This approach uses vector meson dominance

(VMD) to describe the low-Q^2, virtual photon interactions, and Pomeron exchange for the approximate scaling region. It is ideally suited to describe the transition region between large-Q^2 and small-Q^2. This is the kinematic region where the largest differences occur between the NMC and CCFR data sets.

First, we discuss hadron dominance for neutrino deep inelastic scattering [19,20]. The basic physical picture is that the photon or vector boson fluctuates into a quark-antiquark pair before interacting with the nucleus. If the lifetime of such a fluctuation is long enough, a coherent hadronic state can build up before interacting with the target, leading to a shadowing characteristic of hadrons [20,21]. To generalize VMD to neutrino scattering, we have to include both pseudoscalar mesons (pions) and axial vector mesons ($A_1 \cdots$) because of the (V-A) nature of the weak currents.

In order to identify the contributions of the different, virtual hadronic states to the nucleon structure functions, we note that the hadronic tensor for deep inelastic neutrino scattering is defined by

$$W_{\mu\nu}(\nu,Q^2)=\tfrac{1}{2}\sum_S \sum_X \langle PS|J_\mu|X\rangle\langle X|J_\nu|PS\rangle(2\pi)^3\delta^4(P+q-p_X). \tag{5}$$

In Eq. (5), q_ν and ν are the momentum and energy transfer from the neutrino to the nucleon; $Q^2=-q^2$ is the invariant mass of the W-boson; M, P and S are the mass, four-momentum and spin of the target nucleon; p_X is the four-momentum of the final state X. $J_\mu=V_\mu-A_\mu$ is the weak current with vector (V_μ) and axial vector (A_μ) components, respectively. $W_{\mu\nu}$ can be parametrized in terms of six invariant structure functions $W_i(\nu,Q^2)$ in the following form:

$$\begin{aligned}\frac{1}{2M}W_{\mu\nu}(\nu,q^2)=&-g_{\mu\nu}W_1(\nu,q^2)+\frac{P_\mu P_\nu}{M^2}W_2(\nu,q^2)\\&-\frac{i\epsilon_{\mu\nu\alpha\beta}P^\alpha q^\beta}{2M^2}W_3(\nu,q^2)\\&+\frac{q_\mu q_\nu}{M^2}W_4(\nu,q^2)\\&+\frac{P_\mu q_\nu+P_\nu q_\mu}{2M^2}W_5(\nu,q^2)\\&+i\frac{P_\mu q_\nu-P_\nu q_\mu}{2M^2}W_6(\nu,q^2).\end{aligned} \tag{6}$$

In contrast to the vector current, the axial current is not conserved. Thus, we cannot impose current conservation on $W_{\mu\nu}$. In the following, we are interested only in the symmetric, parity conserving piece of the hadronic tensor and want to discuss the major differences between axial and vector currents which are relevant to this work. (More detailed discussions can be found in Refs. [19,20,22].)

Hadronic dominance assumes that the weak current is dominated by intermediate hadronic states coupled to the weak current. The generalization of vector meson dominance to axial vector mesons is straightforward. Here, we quote only the result [19]. The contribution of the vector mesons and axial vector mesons to the structure function $F_2(x,Q^2)=\nu W_2(\nu,Q^2)$ can be written in the familiar form:

$$F_2^{\rm VMD}(x,Q^2)=\frac{Q^2}{\pi}\sum_{V=\rho^+,A_1\ldots}\left(\frac{f_V}{Q^2+m_V^2}\right)^2\sigma_{VN}. \tag{7}$$

Here, f_V are the vector meson coupling constants; m_V are the masses of the vector mesons, σ_{VN} is the vector meson target total cross section. Since the vector mesons couple differently to the electromagnetic and to the weak current, the coupling constants are different in neutrino and charged lepton scattering. Their relative strength can be determined according to the quark counting rules [19]. It turns out that, once the overall weak and electromagnetic coupling constant is removed, the relative coupling of ρ^+ and A_1 to the W-boson ($f_{\rho^+}^2=f_{A_1}^2$) is twice as large as the coupling of the ρ^0 to the photon, $f_{\rho^0}^2$.

The main difference between the axial vector and vector currents is related to the fact that axial currents are only partially conserved (PCAC). Adler's theorem [23] relates the divergence of the axial vector current to the pion field Φ for $Q^2=0$:

$$\partial_\mu A^\mu=f_\pi m_\pi^2\Phi, \tag{8}$$

where $f_\pi=0.93m_\pi$ is the pion decay constant and m_π the pion mass. Imposing this constraint on the hadronic tensor, $W_{\mu\nu}$, we see that only the term containing W_2 survives the limit $Q^2\to 0$ and we obtain the following contribution from PCAC to the structure function $F_2(x,Q^2)$:

$$F_2^\pi(x,Q^2)=\frac{f_\pi^2}{\pi}\sigma_{\pi N}, \tag{9}$$

where $\sigma_{\pi N}$ is the pion nucleon total cross section. However, it is important to note that this is not a consequence of the pion dominance of axial currents. In order to see this, we write the (matrix element of the) axial vector current in terms of the pion-pole term:

$$A_\mu=A'_\mu+f_\pi\frac{q_\mu}{Q^2+m_\pi^2}T^{\pi N\to X}. \tag{10}$$

Here, the second term stands for the contribution of the pion-pole, with $T^{\pi N\to X}$ being the $\pi N\to X$ transition amplitude, and A'_μ the other contributions; for example, the contribution from axial vector mesons. Now comparing this expression with the hadronic tensor, Eq. (6), we immediately see that the pion-pole and its interference terms with A' will only contribute to the structure functions W_4 and W_5, but not to the structure function W_2. Besides, the pionic contributions to the cross section will be proportional to the mass of the outgoing muon, m_μ, because the leptonic tensor is conserved up to terms proportional to m_μ. Thus, the coupling of virtual pions to the axial current is strongly suppressed.

This is a remarkable result. Although the axial current cannot ''emit a pion in the vacuum'' [21], the cross section for neutrino scattering on a nucleon is proportional to the pion cross section on the same target. The observation that the PCAC-term is not to be attributed to the pion-pole, but rather to the longitudinal component of higher mass terms $(A_1\cdots)$ [19], helps to resolve the apparent contradiction. PCAC thus provides a relation between the higher mass contributions to the axial current and the pion cross section. If we identify the PCAC component with the longitudinal part of the A_1, we have the following constraint for the longitudinal cross section:

$$\sigma_L^{A_1N}=\frac{1}{Q^2}\frac{f_\pi^2}{f_{A_1}^2}m_{A_1}^4\sigma_{\pi N}. \tag{11}$$

Inserting Eq. (11) back in Eq. (7), we obtain our final expression for the PCAC-term:

$$F_2^\pi(x,Q^2)=\left(\frac{m_{A_1}^2}{Q^2+m_{A_1}^2}\right)^2\frac{f_\pi^2}{\pi}\sigma_{\pi N}. \tag{12}$$

Since, experimentally, relation (11) does not hold with the A_1 alone, one should include other higher mass contributions. In fact, one should integrate over the whole diffractively produced spectrum, as was pointed out in Ref. [22]. However, if such an integration is performed, Eq. (12) remains a very good approximation for small Q^2-values with a mass which is not exactly the same, but is extremely close to m_{A_1} [22]. The presence of the pion-term for small Q^2 is experimentally well established. Experiments on diffractive meson-production [24], on total cross sections [25] in neutrino- and antineutrino interactions and shadowing [26] in neutrino deep inelastic scattering for very small Q^2 values, have confirmed the validity of PCAC [23].

Finally, it should be noted here that the non-vanishing of the longitudinal cross section for $Q^2\to 0$ in neutrino deep inelastic scattering, as a consequence of PCAC, leads to a ratio $R\equiv\sigma_L/\sigma_T$ which is different from that in muon deep inelastic scattering where current conservation (for vector currents) forces $\sigma_L\to 0$ in the $Q^2\to 0$ limit. In the extraction of the structure function by the CCFR Collaboration, it was assumed that R is the same in both processes. However, this assumption has little effect on the charge ratio, since the pionic contribution does not play a significant role in the kinematic region of the CCFR experiment which is the focus of this paper.

The vector meson undergoes multiple scattering, while traveling through nuclear matter. The resulting shadowing can be calculated using the Glauber multiple scattering expansion [27]. In the eikonal approximation, this gives the following correction to the nuclear structure function [17,18]:

$$A\,\delta^{(V)}F_2^{\nu A}(x,Q^2)=\frac{Q^2}{\pi}\sum_{\rho^+,A_1\cdots}\frac{f_V^2}{(Q^2+m_V^2)^2}\,\delta\sigma_{VA} \tag{13}$$

where

$$\begin{aligned}\delta\sigma_{VA}=&-\tfrac{1}{2}A(A-1)\sigma_{VN}^2\ \mathrm{Re}\int_{z'>z}d^2b\,dz\,dz'\\&\times\exp[ik_L^V(z'-z)]\times\rho^{(2)}(\vec{b},z,z')\\&\times\exp\left(-\frac{A}{2}\int_z^{z'}\frac{d\xi}{L_V}\right)\end{aligned} \tag{14}$$

is the shadowing correction to the vector meson-nucleus cross section with impact parameter $\vec{b}$ and longitudinal momentum transfer to the nucleon $k_L^V=Mx(1+m_V^2/Q^2)$. M, m_V and f_V are the nucleon mass, vector meson masses and vector meson coupling constants, respectively. Further, $\rho^{(2)}(\vec{b},z,z')=N_c\rho(\vec{r})\rho(\vec{r'})$ is the two-body density function, normalized according to $\int d^3r\,d^3r'\,\rho^{(2)}(\vec{r},\vec{r'})=\int d^3r\,\rho(\vec{r})=1$. For the single particle density in iron, we use the Woods-Saxon (or Fermi) density with typical parameters given in Ref. [28]. The mean free path of the vector mesons in the nucleus, L_V, is given by $L_V=[\sigma_{VN}\rho(\vec{b},\xi)]^{-1}$. For the total vector meson cross sections, we use the energy dependent parametrizations of Donnachie and Landshoff [29], $\sigma_{\rho N}=\sigma_{A_1N}=13.63s^{\epsilon}+31.79s^{-\eta}$, where s is the photon-nucleon total center of mass system (c.m.s.) energy, $s=(P+q)^2$, with P and q the four-momenta of the nucleon and photon, respectively. The parameters $\epsilon\approx 0.08$ and $\eta\approx 0.45$ are motivated by Regge theory. Finally, the relative strength of the coupling constants can be determined according to the quark counting rule: $f_{\rho^+}^2:f_{A_1}^2:f_{\rho^0}^2=1:1:\frac{1}{2}$. We use the experimental values for the coupling constants in charged lepton scattering ($f_V\equiv m_V^2/\gamma_V$ and $\gamma_V^2/4\pi=2.0,23.1,13.2$ for $V=\rho^0,\omega,\phi$ [20]) and calculate the coupling of the weak current to the ρ^+ and A_1^+ according to the above relation.

The pionic component, arising through PCAC, will be shadowed in the same way as the vector meson components [21]:

$$A\,\delta^{(\pi)}F_2^{\nu A}(x,Q^2)=\frac{f_\pi^2}{\pi}\left(\frac{m_{A_1}^2}{Q^2+m_{A_1}^2}\right)^2\delta\sigma_{\pi A} \tag{15}$$

where

$$\delta\sigma_{\pi A} = -\tfrac{1}{2}A(A-1)\sigma_{\pi N}^2 \,\mathrm{Re}\int_{z'>z} d^2b\,dz\,dz' \times \exp[ik_L^{\pi}(z'-z)]\times\rho^{(2)}(\vec{b},z,z') \times\exp\left(-\frac{A}{2}\int_z^{z'}\frac{d\xi}{L_\pi}\right), \quad (16)$$

is the shadowing correction to the pion-nucleon total cross section. For the pion-nucleon total cross section, we use $\sigma_{\pi N}=24$ *mbarn* and for the pion decay constant $f_\pi^2=(0.93m_\pi)^2$ [24]. Here we note the following. The appearance of the pion mass in k_L^π has the effect that shadowing in neutrino scattering (at $Q^2\approx 0$) sets in and saturates at much lower energies than in charged lepton scattering, where the coherence condition is governed by the ρ-mass. The early onset of shadowing at low energies has been confirmed experimentally by the BEBC Collaboration [26] and suggests that in neutrino scattering at low Q^2, it is the pion which propagates through the nuclear medium and leads to shadowing. This experimental fact is to be compared to the observation that axial currents cannot emit pions in the vacuum as mentioned above. However, in nuclear medium pions can be diffractively produced as pointed out by Kopeliovich [30]. According to this interpretation, one should also take into account contributions from inelastic shadowing arising from diffractive dissociation of the pions [30]. Since this inelastic shadowing gives only small corrections to the elastic pion contribution, Eq. (16), and the inclusion of the pion component is only important for small $Q^2\sim m_\pi^2$ and negligible for $Q^2\geqslant 1$ GeV^2, in the following, we neglect the tiny contributions from inelastic pion shadowing.

While shadowing due to VMD and PCAC dominates for small Q^2-values, at high virtuality, the interaction between the virtual W-boson and the nucleus is most efficiently parametrized in terms of diffractive scattering through Pomeron exchange. The Pomeron-exchange between the projectile and two or more constituent nucleons models the interaction between partons from different nucleons in the nucleus. The virtual vector boson scatters on one quark in the exchanged Pomeron, leading to a Q^2-dependence which is given by the Q^2-dependence of the Pomeron structure function. Thus, shadowing due to Pomeron exchange is a leading twist effect and survives for large Q^2. The shadowing corrections to the nuclear structure function due to Pomeron exchange can be written as a convolution of the Pomeron structure function, $F_{2\mathbb{P}}$, with the Pomeron flux, $f_{\mathbb{P}/A}$, which describes the number density of the exchanged Pomerons (assuming factorization) [17,18]:

$$A\delta^{(\mathbb{P})}F_2^{\nu A}(x,Q^2)=\int_{ymin}^{A} dy f_{\mathbb{P}/A}(y)F_{2\mathbb{P}}(x_{IP},Q^2), \quad (17)$$

where

$$f_{\mathbb{P}/A} = -A(A-1)\gamma^2 8\pi y^{-1}\,\mathrm{Re}\int_{z'>z} d^2b\,dz\,dz' \times\exp[ik_L^X(z'-z)]\rho^{(2)}(\vec{b},z,z') \times\exp\left(-\frac{A}{2}\int_z^{z'}\frac{d\xi}{L_X}\right). \quad (18)$$

Here, $\gamma^2=\sigma_{pp}/16\pi$ with $\sigma_{pp}=21.7s^{\epsilon}+56.08s^{-\eta}$ the proton-proton total cross section [29], y is the momentum fraction of the nucleon carried by the Pomeron and $x_{\mathbb{P}}=x/y$ is the momentum fraction of the Pomeron carried by the struck quark. y_{min} is given by $y_{min}=x(1+M_{X_0}^2/Q^2)$ with $M_{X_0}^2=1.5$ GeV^2, the minimal mass of the diffractively produced final states. M_{X_0} is chosen such that it is above the relevant vector meson masses in order to avoid double counting. The mean free path of the hadronic state X is $L_X=[\sigma_{XN}\rho(\vec{b},\xi)]^{-1}$ and we assume that the total cross section σ_{XN}, for the state X with the nucleon, is independent of the mass M_X; we take $\sigma_{XN}=25$ *mbarn*. The longitudinal momentum transfer to the nucleon is $k_L^X=My$. $F_{2\mathbb{P}}(x_{\mathbb{P}},Q^2)$ is the structure function of the Pomeron. It contains a $q\bar{q}$ and a triple Pomeron component. These structure functions in Ref. [18] have to be modified in the neutrino induced reaction because of the different coupling of the electromagnetic current and the weak current to the quarks in the Pomeron. In the $q\bar{q}$ component, we replace the factor coming from the charge sum of the quarks $(10+2\lambda_s)/9$ by the factor $4+2\lambda_s$, where the parameter λ_s represents the weaker coupling of the strange quarks to the Pomeron compared to the u and d quarks; we set $\lambda_s\approx 0.5$. In the triple Pomeron term, we replace $F_{2N}^{sea}(x_{\mathbb{P}},Q^2)$ by the structure function appropriate for W exchange:

$$F_2^{(q\bar{q})}(x_{\mathbb{P}},Q^2)=\frac{12(4+2\lambda_s)\beta_0^2}{\sigma_{pp}}\frac{N_{sea}Q^2}{Q^2+Q_0^2}x_{\mathbb{P}}(1-x_{\mathbb{P}}), \quad (19)$$

$$F_2^{(3\mathbb{P})}(x_{\mathbb{P}},Q^2)=\frac{g_{3\mathbb{P}}}{\sqrt{\sigma_{pp}}}F_{2N}^{sea}(x_{\mathbb{P}},Q^2). \quad (20)$$

The parameter $N_{sea}\approx 0.17$ (at $Q^2\sim 4$ GeV^2) is determined by the small x-behavior of the sea density [29]. $g_{3\mathbb{P}}=0.364$ mb$^{1/2}$ and $\beta_0^2=3.4$ GeV^{-2} are the triple Pomeron and quark-Pomeron coupling constants, respectively; $Q_0^2=0.485$ GeV^2 is fixed by matching the photoproduction and deep inelastic regions [31]. The y-dependence of the Pomeron flux is in accordance with recent experimental findings by the H1 [32] and ZEUS [33] Collaborations at Hera from diffractive deep inelastic ep scattering. These results also confirm that the Pomeron structure function contains both a hard and soft component, as had been found by the UA8 Collaboration [34] previously.

The structure function on a heavy target $F_2^{\nu A}$ is given in terms of the proton $F_2^{\nu p}$ and neutron $F_2^{\nu n}$ structure function and the double scattering corrections by

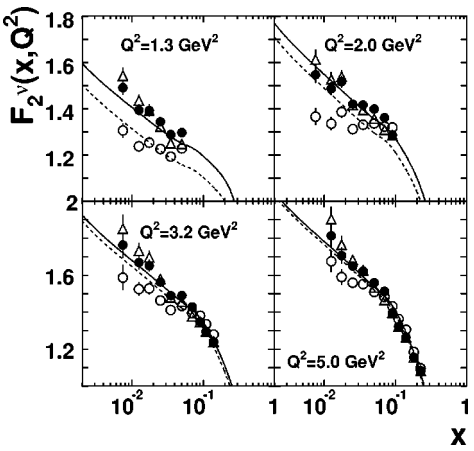

FIG. 2. The CCFR data [1] are shown as a function of x for different Q^2-values together with the parametrization of Ref. [31]. (Data points with higher Q^2-values are not shown.) The solid dots show the data points corrected for heavy target effects using the ''two-phase'' model. The open triangles are corrected using a fit to the heavy target corrections in charged lepton deep inelastic scattering. The open circles represent the uncorrected data points. The solid and dotted curves are calculated with and without the pion contributions, respectively.

$$F_2^{\nu A}=\frac{Z}{A}F_2^{\nu p}+\left(1-\frac{Z}{A}\right)F_2^{\nu n}+\delta^{(\pi)}F_2^{\nu A}+\delta^{(V)}F_2^{\nu A}+\delta^{(\mathbb{P})}F_2^{\nu A}. \tag{21}$$

In the following, we will use this relation with the CCFR data and the calculated shadowing corrections to obtain the structure function on a deuteron target, $F_2^{\nu D}$, which then can be compared to the muon structure function, $F_2^{\mu D}$, on a deuteron target. For the discussion of the ratio $R=F_2^{\nu A}/F^{\nu D}$, we need a parametrization of the neutrino structure functions $F_2^{\nu p}$ and $F_2^{\nu n}$. We will use the parametrization of parton distributions by Donnachie and Landshoff [31] for small Q^2-values and that of the CTEQ Collaboration [16] for large Q^2-values. The parametrization of Donnachie and Landshoff is designed for small Q^2 and matches the deep inelastic and the photo-production regions by taking the behavior of the structure function into account for $Q^2\to 0$. This behavior is parametrized by a multiplicative factor $(Q^2/(Q^2+Q_0^2))^{1+\epsilon}$ which models vector meson dominance for small Q^2. It is clear that the small Q^2-behavior is different for the neutrino structure functions because of the presence of the pion component. However, we expect that the behavior of the non-pionic components should be the same as in muon deep inelastic scattering. Therefore we use the parametrization of Donnachie and Landshoff for the neutrino structure function and add the term F_2^π in order to take into account the effects of PCAC. We checked that this parametrization, with the pionic-term included, describes the CCFR data reasonably well in the small Q^2-region. In Fig. 2 the CCFR data is shown as a function of x for different Q^2-values together with the parametrization of Ref. [31]. The solid dots show the data points corrected for heavy target effects according to Eq. (21), while the open triangles are corrected using a fit to the heavy target corrections in muon deep inelastic scattering. The open circles represent the uncorrected data points. The solid and dotted curves are calculated with and without the pion contributions, respectively. For small Q^2 the pion contributions are relatively large, but with increasingly large Q^2 values the pion contributions become progressively less important.

As far as the similarities and differences between shadowing in neutrino and muon deep-inelastic scattering is concerned, we expect to see the following. In the extremely small Q^2-region, where the hadronic fluctuations of the virtual photon and W-boson dominate the structure functions (pions in the neutrino case and vector mesons in the charged lepton case), shadowing in both cases should be large and should have approximately the same magnitude. On the other hand, for larger Q^2-values, $Q^2\geqslant 1$, the pion contribution becomes negligible and shadowing is largely determined by the vector meson and the Pomeron component. Here, we expect to see some differences due to the different coupling of the weak current to vector and axial vector mesons, compared to the coupling of the electro-magnetic current to vector mesons. More precisely, the relative magnitude of the VMD contribution in neutrino scattering should be roughly half of that in the corresponding charged lepton case. The reason is that, although the coupling is twice as large in the neutrino induced reaction as in the muon induced one, the structure function is larger by about a factor of 18/5. This effect is partly compensated by the A_1, which has the same coupling to the axial current as the ρ^+. However, since the mass of A_1 is large, the A_1 cannot account for the difference. Note also, that the higher mass of the A_1 enters in the coherence condition for shadowing which can be important at the relatively low Q^2-values of the CCFR-data. Finally, at large Q^2-values ($Q^2>10$ GeV^2) where the Pomeron component dominates, there should be no differences in shadowing between neutrino and charged lepton reactions. This is because the relative magnitude of this leading twist component is determined by the coupling of the photon and the W-boson to the quarks in the exchanged Pomeron. This coupling changes in the same way as the structure functions of the nucleons do if we go from charged lepton induced reactions to neutrino induced ones. Thus, differences in shadowing should only occur in the higher twist VMD terms and should show up in the region where shadowing of vector mesons plays a significant role. Since the CCFR data have relatively small Q^2-values ($Q^2\approx 1-15$ GeV^2) in the small x-region, modifications of the shadowing corrections due to vector mesons are expected to be relevant for the CCFR-data.

In order to highlight the similarities and differences between shadowing in charged lepton and neutrino scattering, we calculated the shadowing corrections to the structure functions for both reactions. Since there are experimental data for the ratio between the structure functions of Xenon/deuteron and Ca/deuteron measured for charged lepton scattering by the E665 Collaboration [35] and by the NMC Collaboration [36], we calculated these ratios for both charged lepton and neutrino scattering. The results for the muon induced reaction and their comparison with the experimental data can be found in Ref. [18]. Here, we show them in Figs.

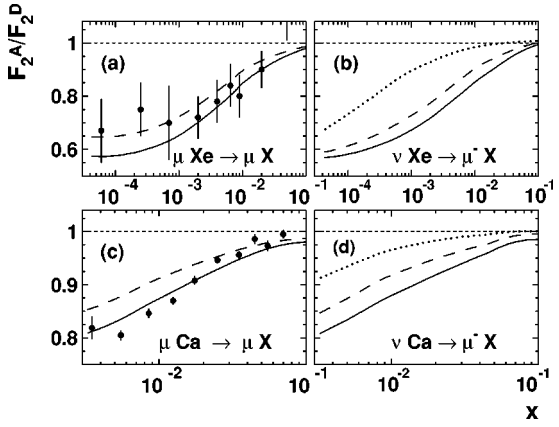

FIG. 3. The ratios F_2^{Xe}/F_2^D and F_2^{Fe}/F_2^D are calculated in the two phase model for charged lepton (a,c) and neutrino deep inelastic scattering (b,d). The dotted and the dashed curves stand for shadowing due to the PCAC component alone, and due to PCAC with VMD contributions also included. The solid curve is the total shadowing. The data are for muon scattering from Ref. [35,36]. For the structure functions we used the parametrization of Ref. [31].

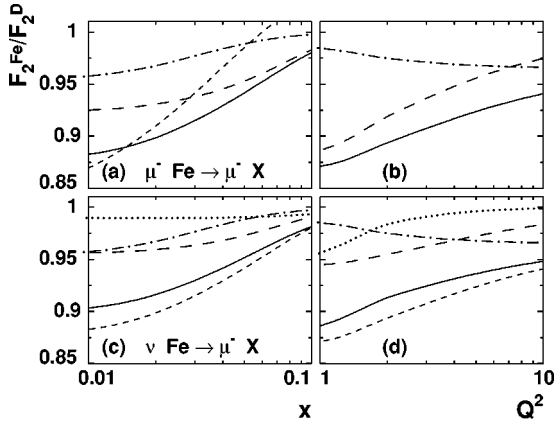

FIG. 4. The different contributions to shadowing on Fe in muon [(a) and (b)] and neutrino [(c) and (d)] deep inelastic scattering as a function of x for fixed $Q^2=3$ GeV^2 [(a) and (c)] and as a function of Q^2 for fixed $x=0.02$ [(b) and (d)]. The dotted, dashed and dash-dotted curves stand for the pion, VMD and Pomeron contributions, respectively. The total shadowing corrections in the muon induced reaction are shown as the short dashed curves in (c) and (d) for comparison. The ''Q^2 independent'' fit is also shown as short dashed curve in (a) for comparison.

3(a) and 3(c) for comparison. While the dashed curves stand for shadowing calculated only with vector mesons, the solid curves also include the Pomeron contributions. We stress that the points are calculated for the x and Q^2-values of the experimental data-points. The experimental data are represented by solid dots with statistical and systematic errors added in quadrature. We note that the calculation describes the experimental data reasonably well and that the important contribution to shadowing comes from VMD in the muon case.

The shadowing corrections in neutrino deep inelastic scattering are shown in Fig. 3(b) for Xe and in Fig. 3(d) for Ca, respectively. Here, the dotted curves are the results with only pion contributions, the dashed with pion and vector meson contributions, and the solid curves include the Pomeron component also and describe thus the total shadowing. We see that the total shadowing in the neutrino induced reaction is comparable in magnitude to shadowing in the charged lepton induced reactions. However, the relative importance of the individual contributions to shadowing are very much different. While the PCAC term dominates in the small x-region, the VMD and Pomeron contributions become more and more important with increasing x (which, in these experiments, is correlated with increasing Q^2) and shadowing is largely determined by their interplay.

Next, we focus on the effects arising from the differences in VMD between the neutrino and the charged lepton case and their relevance to the CCFR data. We calculated the relative contributions of the different components to shadowing on an iron target in the kinematical region of the CCFR experiment. The result is shown in Fig. 4, where the ratio, $R=F_2^{Fe}/F_2^D$, is plotted as a function of x for fixed $Q^2=3$ GeV^2 and as function of Q^2 for fixed $x=0.02$ for neutrino and charged lepton scattering. We see that leading twist shadowing (Pomeron component) is the same for both neutrino and charged lepton induced reactions and is important for high Q^2-values (dash dotted lines). Further, shadowing due to vector mesons is much more significant for charged lepton than for neutrino deep inelastic scattering (dashed lines). In the former, it plays an important role even at relatively high Q^2. Note also that the pion component is negligible above $Q^2>3$ GeV^2. For comparison the ''Q^2 independent'' shadowing is shown in Fig. 4(a) (short dashed line). We see that shadowing for *fixed* Q^2 is not to be described by such a parametrization. This shows the strong Q^2-dependence of shadowing in the available charged lepton data.

Having seen how shadowing in muon deep inelastic scattering compares with shadowing in neutrino deep inelastic scattering, we calculate the shadowing corrections for the CCFR-data on an iron target. We apply these corrections for each data point and integrate over Q^2 (above $Q^2=2.5$ GeV^2) where the CCFR-data [1] and the NMC-data [2] overlap (in order to obtain better statistics) and calculate the ''charge ratio.'' In the non-shadowing region ($x\geqslant 0.07$), we use the Q^2-independent parametrization of F_2^A/F_2^D measured in charged lepton induced processes. The result is shown in Fig. 5 (black circles). The statistical and systematic errors are added in quadrature. The result we would have if we used the Q^2-independent parametrization of the muon shadowing data in the shadowing region is shown as open circles for comparison. The shadowing correction factors are shown as solid and dotted lines for the ''two-phase'' model and the ''Q^2-independent'' shadowing, respectively. The shadowing correction for charged lepton scattering calculated in the ''two-phase'' model is shown as dashed line for comparison. These ratios $R=F_2^{Fe}/F_2^D$ have been obtained according to Eq. (17). While in the neutrino case, we used the data for F_2^{Fe} together with the corrections ($\delta F_2^{\pi}\ldots$) to calculate F_2^D and the ratio R, in the charged lepton case, we used a parametrization for F_2^D and the shadowing corrections to calculate F_2^{Fe} and thus the ratio R. Since the data include points

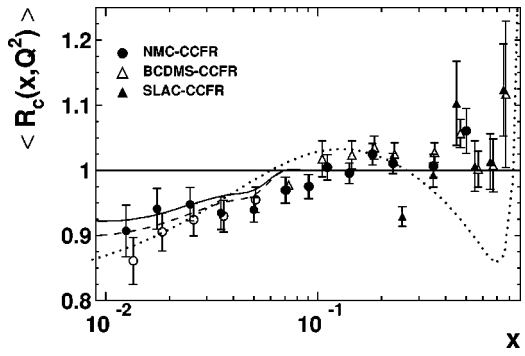

FIG. 5. The charge ratio as a function of x calculated using the CCFR [1] data for neutrino and NMC [2], SLAC [37] and BCDMS [38] data for muon induced structure functions. The data have been integrated above $Q^2=2.5$ GeV^2 over the overlapping kinematical regions and the statistic and systematical errors are added in quadrature. The heavy target corrections are calculated by using the ''two phase-model'' in the shadowing region and a fit to the experimental data on nuclear shadowing in the non-shadowing region (black circles) and by using the Q^2 independent fit in the entire region (open circles). The ratio $R=F_2^{Fe}/F_2^D$ calculated for neutrino and for charged lepton scattering, is shown as solid and dashed lines, respectively. They are calculated in the ''two phase model'' and are averaged over the same Q^2-regions as the data. The Q^2 independent fit is represented by a dotted line.

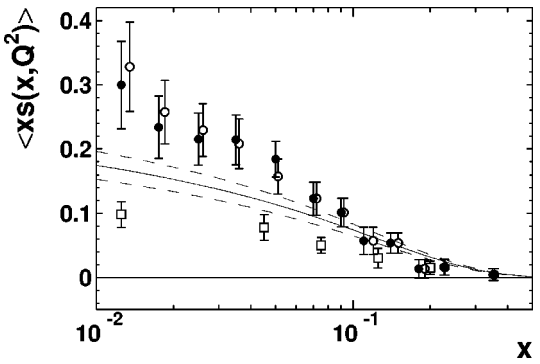

FIG. 6. The strange quark distribution extracted from the CCFR and NMC data assuming the validity of charge symmetry and $s(x)=\overline{s}(x)$. The data have been integrated over the overlapping Q^2 region to obtain better statistics. The solid (open) circles stand for $5/6F_2^{\nu}-3F_2^{\mu}$ using the two phase model (using the Q^2-independent parametrization) for the shadowing corrections. The open boxes stand for the LO CCFR determination of the strange quark density from dimuon production at $Q^2=4$ GeV^2 [39]. The solid line is the NLO CCFR determination at $Q^2=4$ GeV^2 [40]. The band around the NLO curve indicates the $\pm 1\sigma$ uncertainty in the distribution.

with relatively high Q^2-values, we use the parametrization of Ref. [16] (CTEQ4L) for the parton distributions. We also include the data from SLAC [37] and BCDMS [38] for completeness.

The differences between the calculated and ''fitted'' shadowing corrections are partly due to the difference between shadowing in neutrino and muon scattering and partly due to the Q^2-dependence of shadowing, as can be seen in Fig. 5. In connection with the Q^2-dependence, we note that the parametrization of the shadowing corrections has been obtained by fitting the ratio $R=F_2^{\ell A}/F_2^{\ell D}$, in charged lepton deep inelastic scattering. In the small x-region, this fit is mainly determined by the NMC data on Ca [36]. However, the NMC-data for the structure function ratio have lower Q^2-values in the first x-bins than the CCFR-data we use to calculate the charge ratio. The average Q^2 for the NMC ratio $R=F_2^{Ca}/F_2^D$ are $Q^2=1.9,2.5,3.4,4.7$ GeV^2 for $x=0.0125,0.0175,0.025,0.035$, respectively. On the other hand, we integrate the CCFR-data above $Q^2=3.2$ GeV^2 and have $Q^2=4.1,5.5,7.9,9.7$ GeV^2 for the averaged Q^2 values for the same x bins. Since VMD is more important for lower Q^2, it is clear that the parametrization of the NMC-data overestimates the shadowing.

IV. EXTRACTION OF THE STRANGE QUARK DISTRIBUTION

Now that we have determined the shadowing corrections for neutrinos, we can examine how they influence the determination of strange quark densities. Currently, there are two viable methods for the extraction of strange quark parton distributions. The ''direct'' method utilizes charm-hadron production in neutrino deep-inelastic scattering. The triggering signal for this process is the measurement of opposite sign dimuons, one coming from the lepton vertex, while the other comes from the semi-leptonic decay of the charmed hadron [39,40]. The other method is to obtain the strange quark distribution by comparing charged lepton deep inelastic scattering with neutrino deep inelastic scattering. In the second case, the strange quark distribution can be extracted from the relation

$$\frac{5}{6}F_2^{\nu N_0}(x,Q^2)-3F_2^{\mu N_0}(x,Q^2)=xs(x)+\frac{x}{3}[s(x)-\overline{s}(x)]. \tag{22}$$

Equation (22) follows if we assume parton charge symmetry and neglect charm quark contributions. If one assumes that $s(x)=\overline{s}(x)$, the difference between the neutrino and muon structure functions measures the strange quark distribution in the nucleon. Experimentally, the two methods for determining the strange quark distribution are not compatible in the region of small x. This conflict is also reflected in the fact that the ''charge ratio'' R_c is different from one in this region. If we had used the ''correct'' strange quark distribution, the charge ratio would be unity [assuming $s(x)=\overline{s}(x)$].

We converted the CCFR neutrino data on iron to deuteron data by applying our shadowing corrections. We then extracted the strange quark distribution according to Eq. (22). In order to get better statistics, we integrated the structure functions over the overlapping Q^2-regions, as before. The result is shown in Fig. 6, where the strange quark distributions extracted with the ''two-phase'' shadowing and the ''Q^2-independent'' shadowing corrections are shown as black and open circles, respectively. Statistical and systematic errors are added in quadrature. The strange quark distribution as determined by the CCFR Collaboration in dimuon production using a LO analysis [39] is shown as open boxes,

while the distribution extracted in NLO analysis [40] from dimuon data is shown as a solid line. The band around the NLO curve indicates the $\pm 1\sigma$ uncertainty. Although the strange quark distribution obtained from the difference between the neutrino and muon structure functions using the ''two phase'' model for shadowing is smaller in the small x-region than that obtained by applying the Q^2-independent shadowing, both distributions are incompatible with the strange quark distribution extracted from dimuon production.

The remaining discrepancy could be attributed to *different* strange and anti-strange quark distributions [4,5] in the nucleon. From Eqs. (4) and (22) and Fig. 5, we see that the difference $s(x)-\overline{s}(x)$ should be positive for small x-values ($x<0.1$). This is in contradiction with the analysis of Ref. [4], but agrees qualitatively with that in Ref. [5]. Note in this connection that the experimentally determined structure function, F_2^{CCFR}, is a flux weighted average of the neutrino and antineutrino structure functions [1]. Since neutrino events dominate over the antineutrino events in the event sample of the CCFR experiment, it can be approximately regarded as neutrino structure function. In Fig. 7 we extract the strange antiquark distribution vs x using Eq. (22). We use the experimental data for the muon and neutrino structure functions (with our calculated shadowing corrections), together with the strange quark distribution measured in dimuon production. Note that with this method, we obtain a *negative* strange antiquark distribution for small x-values. This strongly suggests that the entire discrepancy cannot be attributed to the difference between $s(x)$ and $\overline{s}(x)$.

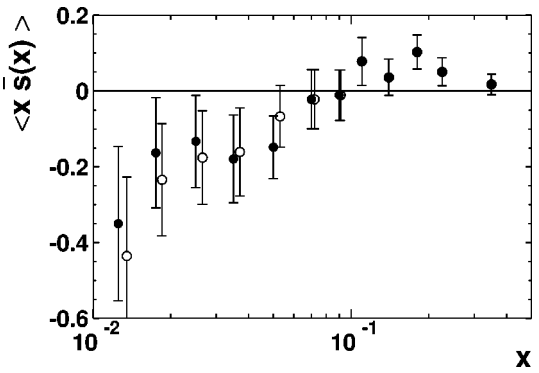

FIG. 7. The (physically unacceptable) anti-strange quark distribution extracted from the data assuming that the discrepancy between the muon and neutrino structure function is due to different strange quark and anti-strange quark distributions and that the strange quark distribution is given by that extracted from di-muon experiments.

V. CONCLUSIONS

In conclusion, we have carefully re-examined shadowing corrections to the structure function F_2^{ν} in deep inelastic neutrino scattering on an iron target. Although the shadowing corrections are not as large as one would naively expect, they are still sizable and similar to shadowing in charged lepton induced reactions in the small-x region. Taking neutrino shadowing corrections into account properly resolves part of the discrepancy between the CCFR neutrino and the NMC muon data in the small x-region. Neutrino shadowing corrections also remove part of the corresponding discrepancy between the two different determinations of the strange quark densities. However, the charge ratio R_c, of Eq. (4), still deviates from unity at small x. Furthermore, the data rules out the possibility that the discrepancy is entirely due to the difference between the strange and anti-strange quark distributions. We are therefore forced to consider the possibility of a rather uncomfortably large charge symmetry violation in the sea quark distributions. This will be discussed in a subsequent paper [41].

ACKNOWLEDGMENTS

We would like to thank S. Brodsky, B. Z. Kopeliovich and W. Melnitchouk for helpful discussions. This work is supported by the Australian Research Council and by the National Science Foundation under contract NSF-PHY-9722706.

[1] CCFR Collaboration, W. G. Seligman *et al.*, Phys. Rev. Lett. **79**, 1213 (1997); Ph.D. thesis, Columbia University, 1997.
[2] NMC Collaboration, M. Arneodo *et al.*, Nucl. Phys. **B483**, 3 (1997).
[3] A. I. Signal and A. W. Thomas, Phys. Lett. B **191**, 205 (1987).
[4] S. J. Brodsky and B. Q. Ma, Phys. Lett. B **381**, 317 (1996).
[5] W. Melnitchouk and M. Malheiro, Phys. Rev. C **55**, 431 (1997).
[6] X. Ji and J. Tang, Phys. Lett. B **362**, 182 (1995).
[7] H. Holtmann, A. Szczurek, and J. Speth, Nucl. Phys. **A596**, 631 (1996).
[8] M. A. G. Aivazis *et al.*, Phys. Rev. D **50**, 3102 (1994).
[9] V. Barone, M. Genovese, N. N. Nikolaev, E. Predazzi, and B. G. Zahkarov, Z. Phys. C **70**, 83 (1996); Phys. Lett. B **317**, 433 (1993); **328**, 143 (1994).
[10] M. Gluck, S. Kretzer, and E. Reya, Phys. Lett. B **380**, 171 (1996); **405**, 391(E) (1997); **398**, 381 (1997).
[11] E. Rodionov, A. W. Thomas, and J. T. Londergan, Mod. Phys. Lett. A **9**, 1799 (1994).
[12] E. Sather, Phys. Lett. B **274**, 433 (1992).
[13] J. T. Londergan and A. W. Thomas, in *Progress in Particle and Nuclear Physics*, edited by A. Faessler (Pergamon, Tübingen, Germany, in press), Vol. 41, pp. 49–124.
[14] C. J. Benesh and T. Goldman, Phys. Rev. C **55**, 441 (1997).
[15] C. J. Benesh and J. T. Londergan, Phys. Rev. C **58**, 1218 (1998).
[16] H. L. Lai *et al.*, Phys. Rev. D **55**, 1280 (1997).
[17] J. Kwiecinski and B. Badelek, Phys. Lett. B **208**, 508 (1988).
[18] W. Melnitchouk and A. W. Thomas, Phys. Lett. B **317**, 437 (1993).

[19] C. A. Piketty and L. Stodolsky, Nucl. Phys. **B15**, 571 (1970).
[20] T. H. Bauer, R. D. Spital, D. R. Yennie, and F. M. Pipkin, Rev. Mod. Phys. **50**, 261 (1978).
[21] Nuclear shadowing in neutrino scattering was first discussed by J. S. Bell in the framework of the optical model. J. S. Bell, Phys. Rev. Lett. **13**, 57 (1964).
[22] B. Z. Kopeliovich and P. Marage, Int. J. Mod. Phys. A **8**, 1513 (1993).
[23] S. L. Adler, Phys. Rev. **135**, B963 (1964).
[24] P. Marage *et al.*, Z. Phys. C **35**, 275 (1987); H. J. Grabosch *et al.*, *ibid.* **31**, 203 (1986); H. Faissner *et al.*, Phys. Lett. **125B**, 230 (1983); E. Isiksal *et al.*, Phys. Rev. Lett. **52**, 1096 (1984); F. Bergsma *et al.*, Phys. Lett. **157B**, 469 (1985).
[25] G. T. Jones *et al.*, Z. Phys. C **37**, 25 (1987).
[26] P. P. Allport *et al.*, Phys. Lett. B **232**, 417 (1989).
[27] R. J. Glauber, Lectures in theoretical physics, Vol. 1, 1958, edited by W. E. Britten and L. G. Dunham (Interscience, New York, 1959).
[28] R. C. Barrett and D. F. Jackson, *Nuclear sizes and structure*, edited by W. Marshall and D. H. Wilkinson (Clarendon, Oxford, 1977).
[29] A. Donnachie and P. V. Landshoff, Phys. Lett. B **296**, 227 (1992).
[30] B. Z. Kopeliovich, Phys. Lett. **27B**, 461 (1989).
[31] A. Donnachie and P. V. Landshoff, Z. Phys. C **61**, 139 (1994).
[32] H1 Collaboration, T. Ahmed *et al.*, Phys. Lett. B **348**, 681 (1995).
[33] ZEUS Collaboration, M. Derrick *et al.*, Z. Phys. C **38**, 569 (1995); J. Breitweg *et al.*, Eur. Phys. J. C **1**, 81 (1998).
[34] UA8 Collaboration, A. Brandt *et al.*, Phys. Lett. B **297**, 417 (1992).
[35] E665 Collaboration, M. R. Adams *et al.*, Phys. Rev. Lett. **68**, 3266 (1992).
[36] NMC Collaboration, P. Amaudruz *et al.*, Z. Phys. C **51**, 387 (1991); Phys. Rev. Lett. **66**, 2712 (1991); Phys. Lett. B **295**, 159 (1992).
[37] L. W. Whitlow, Ph.D. thesis, Stanford, 1990.
[38] BCDMS Collaboration, A. C. Benvenuti *et al.*, Phys. Lett. B **237**, 592 (1989).
[39] S. A. Rabinowitz *et al.*, CCFR Collaboration, Phys. Rev. Lett. **70**, 134 (1993).
[40] CCFR Collaboration, A. O. Bazarko *et al.*, Z. Phys. C **65**, 189 (1995).
[41] C. Boros, J. T. Londergan, and A. W. Thomas, Phys. Rev. Lett. (to be published), hep-ph/9805011.